JOURNAL OF PROPULSION AND POWER
Vol. 23, No. 5, September–October 2007

Three-Dimensional Nonreflecting Boundary Conditions for Swirling Flow in Turbomachinery

Pierre Moinier* and Michael B. Giles†
Oxford University, Oxford, OX1 3QD England, United Kingdom
and
John Coupland‡
Rolls-Royce, plc., Derby, DE24 8BJ England, United Kingdom

DOI: 10.2514/1.22117

This paper discusses the implementation of nonreflecting boundary conditions for the computation of linear unsteady aerodynamic turbomachinery problems. Based on the use of precalculated far-field acoustic eigenmodes for a mean flow that is assumed to be uniform axially and circumferentially, but nonuniform in the radial direction, the method very effectively reduces the reflections and improves the convergence rate for both inviscid and viscous flows. Extension of the implementation within a generalized minimal residual method is summarized and convergence results are presented. This is the companion paper of a previous publication that addressed the numerical computation of the eigenmodes and their use for postprocessing.

I. Introduction

THERE are different approaches to analyze turbomachinery unsteadiness. These methods vary from the use of linearized flow solvers based on the observation that the unsteadiness is sufficiently small to be considered a linear perturbation to a steady flow, to fully nonlinear 3-D unsteady methods. Among all of these, the linear harmonic Euler and Navier–Stokes methods have become very popular in industry, due to a successful compromise between accuracy and computational cost, and constitute the background to this paper.

Whatever the method used and the problem under investigation, the numerical solution is calculated on a truncated finite domain, and one must prevent any nonphysical reflections of outgoing waves at the far-field boundaries that could contaminate the numerical solution. This becomes essential in turbomachinery applications in which the boundaries are often not very far from the blades, because the physical spacing between the blade rows can be quite small. It therefore becomes highly important for an accurate simulation to construct nonreflecting boundary conditions (NRBCs).

Preventing spurious reflections that would corrupt the solution is not only important to get an accurate prediction of the flowfield, but also to get more efficient computations; convergence rate is enhanced due to an improvement of the transmission of outgoing waves, allowing smaller meshes to be used.

There is already a very broad and diverse existing theory for different applications. In computational fluid dynamics (CFD), the most common techniques employed use an analytical approach to describe the eigenmodes of the governing equations. In 1975, Adamczyk et al. [1] constructed exact NRBCs for the potential equation when calculating linearized unsteady flows by matching the known analytical solution with the computed one. Extended by Hall and Crawley [2] to the linearized Euler equations, Giles [3], in 1990, introduced exact nonreflecting 2-D boundary conditions based on the ideas of Engquist and Majda [4], using a characteristic analysis of the linearized equations. Later, Saxer and Giles [5] extended the steady NRBCs into a quasi-3-D formulation, assuming the circumferential variation is much larger than the radial variation, and successfully applied it to the solution of axial turbine stages. Finally, in 1996, Fan and Lakshminarayana [6] followed the same approach for unsteady flows and demonstrated their effectiveness for turbine calculations. In the field of computational aeroacoustics, people have developed other approaches based either on the discrete system-building numerical NRBCs (e.g., Rowley and Colonius [7]) or on asymptotic expansions (e.g., Grote and Keller [8] and Tam [9]).

In this paper, we are interested in solving complex turbomachinery problems in which the radial variations in the mean and unsteady perturbation flowfields cannot be ignored. For that purpose, we intend to resume a theory described by Lorence et al. [10], who generalized Giles's [3] approach to the 3-D Euler equations using a mixed analytical and numerical method to approximate the 3-D eigenmodes. In their paper, Hall et al. [10] demonstrated the effectiveness of their method to eliminate the reflections at the boundaries through the visualization of pressure contours that were shown to pass smoothly out of the computational domain. The test case simulated the flow through a cascade of cambered airfoil and is known as the tenth standard configuration [11]. The present study addresses the extension of the approach to the 3-D Navier–Stokes equations.

The primary objective is to determine the appropriate acoustic eigenmodes for a swirling axisymmetric mean flow using numerical eigenvalue and eigenvector computations and use them throughout the calculation to enforce NRBCs. The first key step is to compute a numerical approximation to the eigenmodes for linear unsteady flow perturbations superimposed upon an inviscid/viscous mean flow, which is swirling and axisymmetric.

To achieve this, a preprocessor tool solving the linear 3-D cylindrical Euler/Navier–Stokes equations was developed using LAPACK, a general-purpose numerical linear algebra library.[§] Because of the axisymmetry of the mean flow, the eigenmodes are Fourier modes circumferentially. Considering each Fourier mode separately and discretizing the relevant ordinary differential equation in the radial direction, the eigenvalues of the resulting matrix give the complex axial wave number, and the corresponding right and left eigenvectors give the eigenmodes of the partial differential equation. The complex axial wave number is used to decompose the flowfield into upstream and downstream traveling eigenmodes, whereas the

Received 29 December 2005; revision received 8 March 2007; accepted for publication 11 April 2007.

*Research Officer, Computing Laboratory; moinier@comlab.ox.ac.uk.
†Professor, Computing Laboratory; giles@comlab.ox.ac.uk. Member AIAA.
‡Aerothermal Methods Specialist, P.O. Box 31.

§Data available online at http://www.netlib.org/lapack [retrieved 24 July 2007].

eigenvectors are used to measure the amplitude of the outgoing modes and to set the appropriate values for the flow quantities at the boundaries of the computational domain to prevent any reflections. In a previous paper, Moinier and Giles [12] described how these eigenmodes can be computed and sorted, depending on whether they are acoustic, entropy, or vorticity modes. They also discussed the implementation issues and validated their results with analytical formulations for both inviscid and viscous cases before applying them to postprocess the computed flowfield and demonstrate the need for NRBCs. The present paper constitutes the second step in this study, by applying the theory to a CFD code to remove the unphysical reflections.

The paper starts with a brief review of the eigenmode analysis followed by the implementation within a standard 3-D linear harmonic Navier–Stokes solver and its stabilized version via the generalized minimal residual method (GMRES). To exemplify the nonreflective character of the approach, three 3-D test problems are considered: a benchmark problem consisting of an annular cascade of flat-plate stator vanes placed in a parallel annulus duct (known as the category-4 benchmark problem [13]) and two viscous turbine outlet-guide-vane (OGV) test cases.

II. Eigenmode Analysis

The eigenmode analysis can be performed for both inviscid and viscous problems. When the Euler equations are linearized to consider small unsteady perturbations to a mean flow, which is axially and circumferentially uniform but varies radially, the eigenmodes are of the form $Q(r,\theta,z,t) = e^{\mathrm{i}(\omega t + m\theta + kx)}\mathrm{u}(r)$, where Q is a five-dimensional vector for which the components are the density; the axial, radial, and circumferential velocity components; and the pressure; $\mathrm{u}(r)$ is a radially varying column vector; and ω is a known quantity corresponding to either the frequency of an incoming wave (forced response) or a blade-vibration frequency (flutter). The discretization on a radial grid of the equation that arises after substitution of these solutions results in the general eigenvalue problem (GEP) that is solved. The viscous eigenmodes are solutions of a similar GEP, to which viscous flux terms were added. In both cases, appropriate symmetry conditions are enforced at the centerline $r = 0$ for cylindrical ducts and slip/no-slip conditions are imposed on the velocity at solid walls. All the details of the analysis can be found in [12].

To solve the GEP, a representation of the mean flow quantities must be computed at each predefined radial mesh point at which the discretization occurs. This is achieved via a simple circumferential average of an already converged 3-D steady solution. It is also assumed that the mean flow is axial (i.e., the steady velocity has no radial component $U_r = 0$) meaning that the model problem can only be suitable for geometries with parallel endwalls (see the Appendix). Geometries without parallel end walls will not fulfill this condition, but nevertheless, the same procedure is applied, with an extra correction added at the end of this process. First, all mean radial velocity components U_r are set to zero and the eigenmodes are computed. The radial velocity components present in the eigenmodes are then corrected to satisfy the endwall angles. Technically, if α denotes this angle, then $\tan(\alpha) = U_r/U_x$, and if u_x denotes the axial velocity perturbation, then the velocity perturbation u_r is replaced by the linear combination $u_r^* = u_r + \tan(\alpha)u_x$, so that the corrected perturbation has the property that $u_r^* = \tan(\alpha)u_x$ on the endwall.

Each eigenmode can be identified as belonging to one of four categories: upstream and downstream-propagating acoustic modes and downstream-propagating entropy and vorticity modes. To distinguish between the different families, it is necessary to look at the eigenvectors of density ρ, velocity, and pressure p perturbations at the different radial positions. A sorting process was devised, relying 1) on the sign of the imaginary part of their wave number to separate the upstream-propagating acoustic modes from the others, 2) on the evaluation of which modes, among those remaining, have the largest pressure perturbation $||\rho||^2$ and discarding them, and 3) on which modes, among those remaining, have the largest entropy perturbation $||\rho - c^2\rho||^2$. For a complete description, the interested reader is urged to refer to [12].

III. Nonreflecting Boundary Conditions

In this section, the details of the NRBC treatment are presented for a calculation on a single blade row consisting of N identical blades. Because of the axisymmetric assumption, it will only be applied at the inlet and outlet of a geometry truncated to a single blade-to-blade passage of angular width $\Delta\theta = 2\pi/N$. An interblade phase angle β is introduced to take into account the phase shift that may exist at neighboring blades.

A. Implementation for Standard Applications

Under the same assumptions, a general unsteady flow solution of the linearized Navier–Stokes equations with a given frequency ω can be decomposed into a sum of eigenmodes:

$$\mathbf{Q}(x,r,\theta,t) = \sum_{m,n} a_{mn} \exp\left(\mathrm{i}\omega t + \mathrm{i}p_m \frac{\theta}{\Delta\theta}\right)\mathbf{u}_{mn}(r) \tag{1}$$

where $p_m = \beta + 2\pi m$. For the case of a rotor subject to forced response due to a neighboring row of stators, we will have

$$\frac{p_m}{\Delta\theta} = \frac{p_m}{\Delta\theta_r} = \frac{1}{\Delta\theta_r}(\beta + 2\pi m) = \frac{\beta}{\Delta\theta_r} + N_r m$$
$$= \frac{N_s 2\pi}{N_r \Delta\theta_r} + N_r m = N_s + mN_r \tag{2}$$

We recognize the same definition of the acoustic modes as that given by Tyler and Sofrin [14] for uniform axial flow in cylindrical and annular duct and for which they developed an analytical description, valid as long as the mean flow has no swirl.

Equation (1) consists of a double summation over the circumferential mode number p_m of Fourier mode m and the radial modes n that exist for each value of m. The modal amplitude a_{mn} will be proportional to $e^{\mathrm{i}k_{mn}x}$, where k_{mn} is the axial wave number.

Given an unsteady flow solution $\mathbf{Q}(x,r,\theta,t)$ computed by a linear harmonic method, we can, under the condition that the field is periodic, Fourier transform it at each specified radial position of the boundary along the predefined circumferential lines of length $\Delta\theta$ and write that

$$\mathbf{Q}(x,r,\theta,t) = \sum_m \hat{\mathbf{Q}}_m(x) e^{\mathrm{i}p_m \frac{\theta}{\Delta\theta}} \tag{3}$$

where

$$\hat{\mathbf{Q}}_m(x) = \frac{1}{\Delta\theta}\int_{\theta_1}^{\theta_2} \mathbf{Q}(x,r,\theta,t) e^{-\mathrm{i}p_m \frac{\theta}{\Delta\theta}}\,\mathrm{d}\theta \tag{4}$$

As stated in Eq. (1), the unsteady solution can exactly be represented by a summation over circumferential and radial modes. It is therefore possible to approximate this solution by sorting and keeping the dominant modes, the level of accuracy depending on the identification process and the number of modes retained.

Suppose now that the eigenmodes $\mathbf{u}_{mn}$ have already been sampled at a discrete set of radial points, forming the columns of a matrix E_m, we then have

$$\hat{\mathbf{Q}}_m(x) = E_m \mathbf{a}_m \tag{5}$$

where $\mathbf{a}_m$ is the vector of modal amplitudes for different radial modes corresponding to circumferential mode m. If the number of radial eigenmodes kept to approximate the unsteady solution is chosen so that E_m is a square matrix, then this can be inverted to obtain

$$\mathbf{a}_m = (E_m)^{-1}\hat{\mathbf{Q}}_m(x)$$

giving the modal amplitude for each m and n.

In the case of flutter, the linear solution at the inflow or outflow boundary should only consist of outgoing waves. Any incoming

component present in the converged solution can only be due to numerical reflections. At the upstream boundary (located at $x = x_{\text{in}}$), the outgoing modes are those that are propagating upstream. Assuming that the dominant outgoing eigenmodes were identified and stored as the column of the matrix E_m^{ups}, the outgoing component $\mathbf{Q}^{\text{out}}$ for each mode m can be found as

$$\hat{\mathbf{Q}}_m^{\text{out}}(x_{\text{in}}) = E_m^{\text{ups}}(E_m^{-1}\hat{\mathbf{Q}}_m)$$

To minimize memory requirements, the downstream-propagating component at the downstream boundary (located at $x = x_{\text{out}}$) is obtained by subtracting the upstream-propagating component so that it gets computed by

$$\hat{\mathbf{Q}}_m^{out}(x_{out}) = \{\hat{\mathbf{Q}}_m(x_{out}) - E_m^{ups}[(E_m)^{-1}\hat{\mathbf{Q}}_m(x_{out})]\},$$

where E_m^{ups} is the matrix of dominant outgoing eigenmodes, computed at the downstream boundary.

Upstream and downstream boundaries are both handled through fluxes calculated through the boundary faces using a standard 1-D characteristic treatment and incorporating prescribed flow information Q_{ext}, which initially is identically zero. To suppress the reflections and make sure that all outgoing waves leave the computational domain smoothly, the flow on the exterior of the boundaries is set to be equal to the sum of the outgoing modes; in other words, Q^{out} is used to update Q_{ext} and create a new state for the computation of the fluxes. This is essentially an intelligent NRBC extrapolation to the ghost node at which Q_{ext} is defined.

In practice, to avoid stability problems, a relaxation parameter σ was introduced to slowly modify the exterior state. The updating process that is applied at each iteration may generically be expressed as

$$(\mathbf{Q}_{\text{ext}}^{\text{new}})^{j+1} = (\mathbf{Q}_{\text{ext}}^{\text{old}})^{j} + \sigma\left(\sum_m [\hat{Q}^{\text{out}} - (\hat{\mathbf{Q}}_{\text{ext}}^{\text{old}})^{j}]_m e^{ip_m \frac{\theta}{\Delta\theta}}\right) \quad (6)$$

In the case of forced response, the only difference is due to the presence of a prescribed incoming disturbance that is first subtracted from the boundary-flow data Q_{ext} and the result is Fourier-transformed. The determination of the outgoing component remains the same as for the flutter problem, and the incoming disturbance is added back once the summation over the circumferential modes m was computed. The updating process applied at each iteration becomes

$$(\mathbf{Q}_{\text{ext}}^{\text{old}})^{j} := (\mathbf{Q}_{\text{ext}}^{\text{old}})^{j} - Q_{\text{presc}}$$

$$(\mathbf{Q}_{\text{ext}}^{\text{new}})^{j+1} := (\mathbf{Q}_{\text{ext}}^{\text{old}})^{j} + \sigma\left(\sum_m [\hat{Q}^{\text{out}} - (\hat{\mathbf{Q}}_{\text{ext}}^{\text{old}})^{j}]_m e^{ip_m \frac{\theta}{\Delta\theta}}\right) + Q_{\text{presc}}$$

where Q_{presc} denotes the prescribed incoming disturbance. Although no thorough parametric study was carried out, $\sigma = 0.1$ was found to be a good value and is used for all cases.

B. Implementation Within a GMRES Stabilization Procedure

Usually, the standard linear code converges without difficulty. However, pathological cases were encountered when the steady flow calculation enters in a low-level limit cycle, failing to converge to a steady state. Campobasso and Giles [15] related these problems to physical phenomena such as vortex shedding at a blunt trailing edge, unsteady shock/boundary-layer or shock/wake interaction. For many aeroelastic analyses, these small unsteady phenomena in the base flow are not significant, and they achieved stable computations through the use of GMRES. The resulting stabilized code became the default for cases with convergence problems, and so it was necessary to extend the nonreflecting treatment to the GMRES solver.

The key idea behind the GMRES stabilization algorithm is to consider the linearized harmonic Navier–Stokes equations as a simple linear system of the form

$$A\mathbf{x} = \mathbf{b}$$

and to regard the code for its solution as the fixed-point iteration

$$\mathbf{x}^{j+1} = (I - M^{-1}A)\mathbf{x}^{j} + M^{-1}b \quad (7)$$

in which M^{-1} is a preconditioning matrix resulting from the Runge–Kutta time-marching algorithm, a Jacobi preconditioner, and one multigrid cycle. More details may be found in [15]. For this particular type of problem, the right-hand side, generically viewed as $\mathbf{b}$, includes the boundary-condition data (the incoming wake for the case of forced response) and is set to zero during the evaluation of the Krylov vectors. In the case of the nonreflecting boundary-condition treatment, the boundary data are no longer constant and must be considered as part of the unknowns within the GMRES solver. As a consequence, and considering the updating process of the boundary-flow data, as expressed in Eq. (6), the fixed-point iteration (7) becomes

$$\begin{pmatrix} \mathbf{Q} \\ \mathbf{Q}_{\text{ext}} \end{pmatrix}^{j+1} = \begin{bmatrix} (I - M^{-1}A) & K \\ \sigma F^{-1}H & (1-\sigma)I \end{bmatrix} \begin{pmatrix} \mathbf{Q} \\ \mathbf{Q}_{\text{ext}} \end{pmatrix}^{i} + \begin{pmatrix} M^{-1}b \\ 0 \end{pmatrix}$$

where K denotes the operations performed at the boundaries H, those that are performed to compute $\hat{\mathbf{Q}}^{\text{out}}$, and F^{-1} is the inverse Fourier transform. With this slight change in mind, the algorithm presented by Campobasso and Giles [15] extends itself naturally to take into account the extra unknown $\mathbf{Q}_{\text{ext}}$ added in the Krylov vectors.

IV. Storage and Extra CPU Requirement

The approximate eigenmodes computed during a preprocessing step are stored in separate files and read at the beginning of a run, increasing the original memory requirement. If N_c and N_r denote, respectively, the number of circumferential lines and the number of radial eigenmodes kept for each N_m circumferential mode, then the dimension of the eigenvector arrays is $5N_cN_rN_m$. In practice, $N_m = 5$ and $3 \le N_r \le 10$ $N_c \le$ the number of radial grid lines. With N_c never bigger than 100, this gives a total of less then 1 MB per array. The extra operations required at each iteration are $\mathcal{O}(N_c^2 N_r N_m)$ and hence negligible compared with the flux evaluations and other operations performed, as long as N_c, N_r, and N_m are kept reasonably low. Profiling the code shows that the NRBC treatment is responsible for less than 0.5% of the total CPU cost.

V. Postprocessing

The nonreflecting boundary-condition treatment is based on the determination of the eigenmodes that correspond to downstream or upstream-propagating waves, and the differentiation between the directions of propagation is achieved using a sorting procedure of the eigenvalues of the eigenmode analysis. Noting that such a decomposition can be performed not only at the far-field boundary but also anywhere inside the computational domain, this gives a rather straightforward method to split the unsteady flowfield into acoustic propagating waves and to follow the behavior of a particular eigenmode. The same procedure performed on the solution obtained with the regular boundary treatment and then on the solution obtained with the NRBC treatment will show the effectiveness of the nonreflecting treatment. Although the plot will only show the gain relative to a certain set of eigenmodes, it will be a good measure of the results achieved, because all the dominant eigenmodes are involved in the process. For a more complete description, the interested reader should refer to [12].

VI. Results

The nonreflecting boundary conditions are first demonstrated for the case of an inviscid uniform axial flow. The problem consists of vortical wakes impinging on an axially aligned flat plate in a parallel annular duct [13]. The CFD calculation was performed using the HYDRA nonlinear and linear codes (see Moinier [16] and Duta [17]) on a uniform $113 \times 33 \times 65$ grid (Fig. 1), with conventional 1-D nonreflective boundary conditions followed by the new approach.

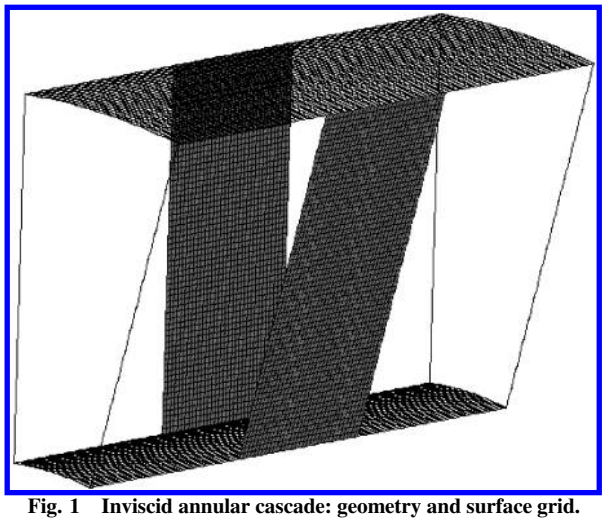

Fig. 1 Inviscid annular cascade: geometry and surface grid.

The results in Fig. 2 show the sound-pressure level (SPL[¶]) evaluated at the outer wall of the duct for the first radial harmonic of a standard linear computation for Fourier modes −32, −8, 16, 40, and 64. The incident wave corresponds to circumferential mode 16. Because there are 24 blades in the cascade, the interaction generates a response solely in modes $16 + 24m$ for integer m.

The harmonic decomposition shows a combination of both propagating and evanescent modes upstream and downstream of the flat plate located at $0 < x < 0.1$. The modes with approximately constant amplitude are the cuton propagating modes; analytically, their amplitudes should be perfectly constant. The modes with amplitudes that appear to be almost linear in this logarithmic plot are the cutoff evanescent modes; their linear logarithmic behavior corresponds to the expected exponential decay of the modes. The most important point of interest is that the unsteady interaction produces a mode −8 downstream-propagating acoustic wave which is reflected at the downstream boundary into a mode −8 upstream-propagating acoustic wave. There is also a very strong reflection in Fourier mode 16; in this case, this is a consequence of the outgoing vortical mode, which is not plotted. The reflected mode decays very rapidly away from the boundary and so does not contaminate the computed solution in the neighborhood of the blade. In Fig. 2b, the same decomposition is plotted, but on a solution in which the 3-D nonreflecting boundary conditions have been used. The strong upstream reflection of mode −8 was largely reduced and the one in Fourier mode 16 was eliminated. These results are in agreement with those obtained by Wilson [18], who applied a similar technique to reduce the reflections at the boundaries.

The second example, provided by Rolls-Royce, concerns the unsteady viscous flow around a turbine OGV, shown in Fig. 3, due to an incoming acoustic wave in Fourier mode −10. Figure 4a shows the SPL of the first radial harmonic for Fourier modes −28, −10, 8, and 26 when using standard quasi-1-D nonreflecting boundary conditions. All of the acoustic modes are cuton upstream and downstream of the blade located in the region $0.64 < x < 0.84$. Downstream of the blade, there are four acoustic modes propagating downstream and two propagating back upstream, as a result of spurious reflections. These reflections are in the two higher circumferential harmonics, for which the quasi-1-D nonreflecting boundary conditions are much less effective. Upstream of the blade, there are three modes propagating upstream and two propagating downstream, one of which is the original input disturbance and the other is another spurious reflection. Figure 4b shows the great improvement that is achieved through the use of 3-D nonreflecting boundary conditions. There is now no spurious reflection at either the inflow or the outflow boundaries.

A comparison of the OGV convergence histories is presented in Fig. 5, in which the effects of the new boundary treatment are

[¶]Twenty times the logarithm to the base 10 of the ratio of rms sound pressure to the reference sound pressure.

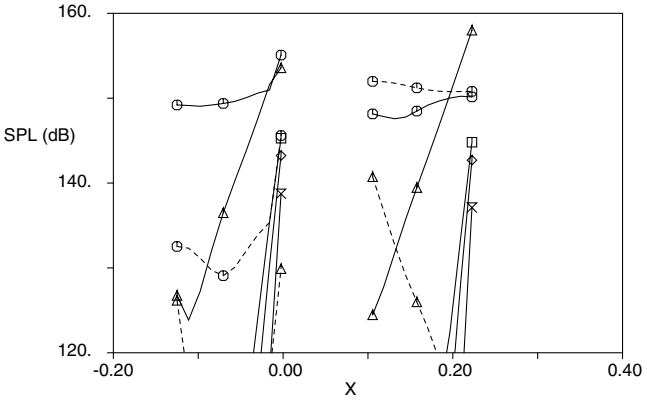

a) Quasi-1-D nonreflecting boundary conditions

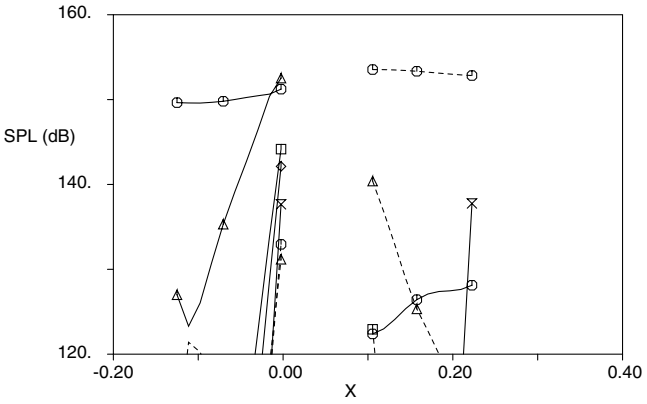

b) 3-D nonreflecting boundary conditions

Fig. 2 Inviscid annular cascade: amplitude of the first radial harmonic acoustic mode propagating upstream (solid line) and downstream (dashed line) for circumferential Fourier modes; ◇: −32, ○: −8, △: 16, ×: 40, and □: 64.

compared with those obtained with the standard treatment. Generally speaking, the NRBCs improve the convergence rate, particularly when these are enforced at each iteration, that is, $itr = 1$ (when applied at every 10 iterations, that is, $itr = 10$, the gain is almost not noticeable). Convergence can be enhanced by using GMRES, even though the test case does not present any stabilization problems. For this study, using 20 Krylov vectors yields computational savings of about 30% in asymptotic convergence (between residuals levels of 10^0 and 10^{-12}) and slightly more than 50% in initial convergence (between residuals levels of 10^0 and 10^{-4}). One should note that more refined results could probably be obtained after a parametric study to find the optimal value of σ and that increasing the number of Krylov vectors will always improve the convergence rate, with an upper limit fixed, however, by the available computing resources.

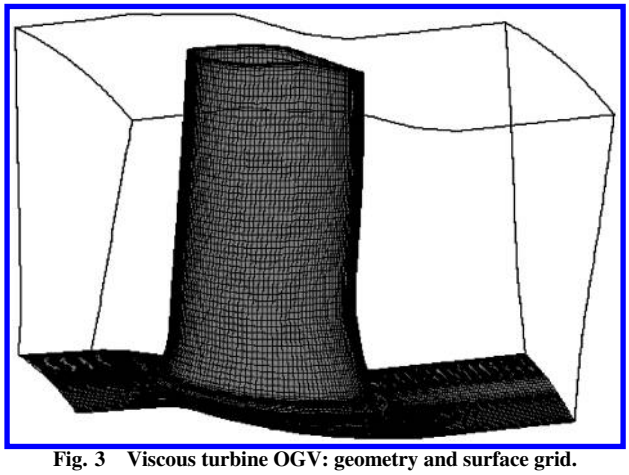

Fig. 3 Viscous turbine OGV: geometry and surface grid.

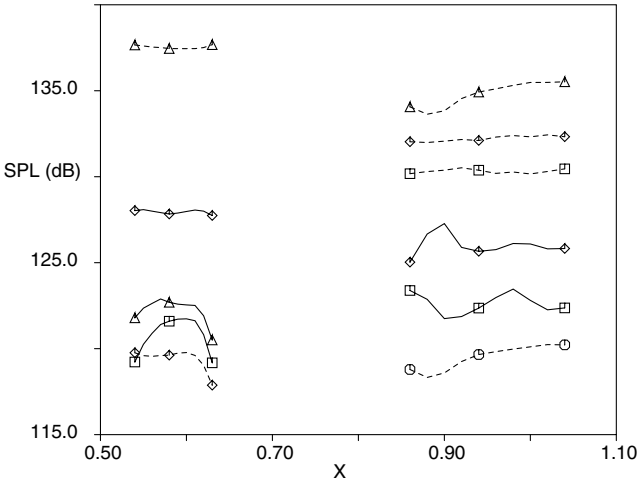

a) Quasi-1-D nonreflecting boundary conditions

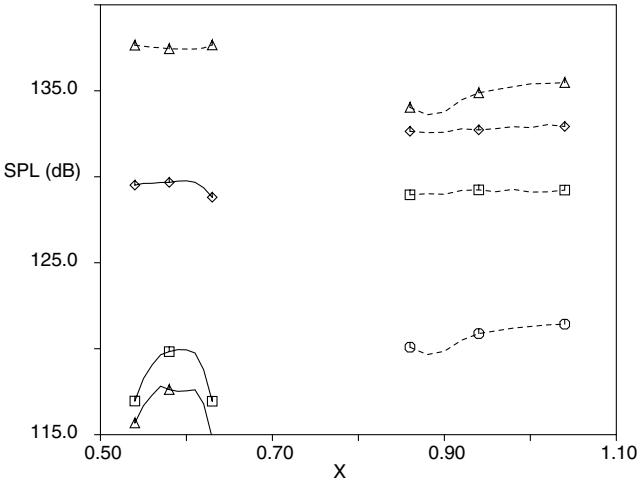

b) 3-D nonreflecting boundary conditions

Fig. 4 Viscous turbine OGV: amplitude of the first radial harmonic acoustic mode propagating upstream (solid line) and downstream (dashed line) for circumferential Fourier modes;◇: −28, △: −10, ○: 8, and □: 26.

A last example illustrating the successful application of the 3-D nonreflecting boundary conditions to a real turbomachinery flow consists of the unsteady viscous flow in the region of another bypass-duct OGV, this time as a result of the interaction with the wakes shed by the upstream fan blades. Figure 6 shows the OGV and the incoming wake perturbation on the OGV inlet plane. The fan stage under consideration consists of 26 rotor blades and 58 vanes. Results are presented at a speed representative of cutback operation at twice

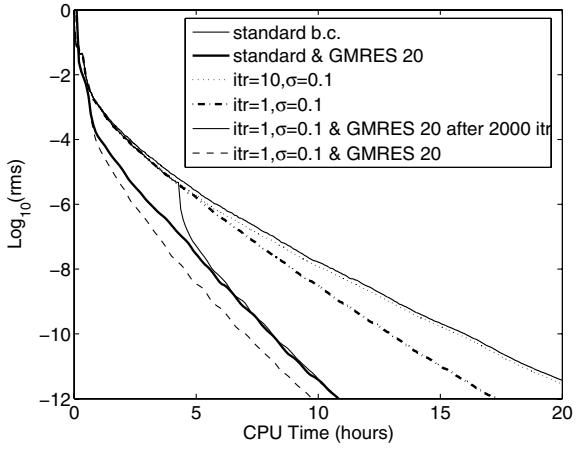

Fig. 5 Turbine OGV: convergence history comparisons.

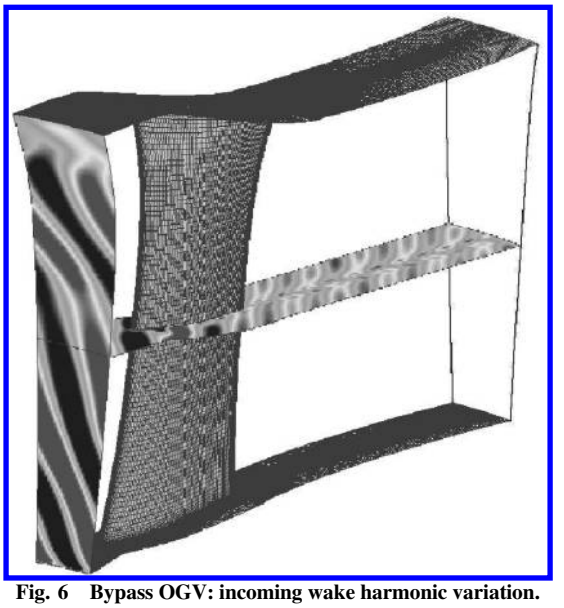

Fig. 6 Bypass OGV: incoming wake harmonic variation.

the rotor-blade-passing frequency. At these conditions, only acoustic modes in circumferential Fourier modes −6 and 52 are cuton.

The casing SPL levels of radial harmonics 1 and 5 for circumferential Fourier mode −6 downstream of the OGV are plotted against axial distance in Fig. 7. The eigenmode analysis was conducted for the radially nonuniform swirling flow downstream of the OGV. The beneficial effects of the 3-D nonreflecting boundary-condition treatment in attenuating spurious reflections from the boundaries is particularly apparent for the higher radial harmonic, in which simple quasi-1-D nonreflecting boundary conditions lead to the nonphysical situation of the amplitude of the reflected wave being greater than the transmitted wave. The averaged (over the region $0.29 < x < 0.39$) SPL values for each cuton radial harmonic at circumferential Fourier mode −6 are presented in Fig. 8. The improvement due to the use of 3-D nonreflecting boundary conditions is evident for all the cuton radial harmonics. A similar type of analysis was conducted for several harmonics of the blade-

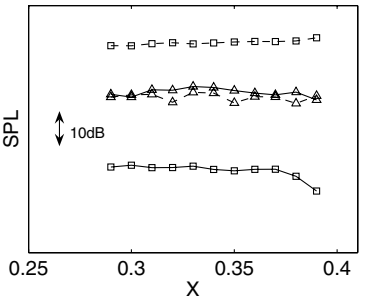

a) Quasi-1-D nonreflecting boundary conditions

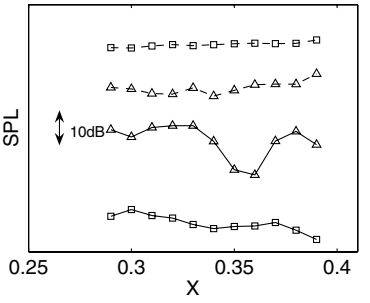

b) 3-D nonreflecting boundary conditions

Fig. 7 Amplitude of radial harmonics in $m = -6$ downstream of OGV; □: radial harmonic 1, △: radial harmonic 5, dashed line: transmitted (downstream), and solid line: reflected (upstream).

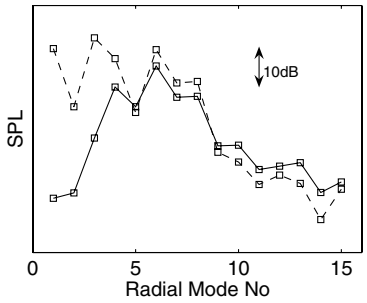

a) Quasi-1-D nonreflecting boundary conditions

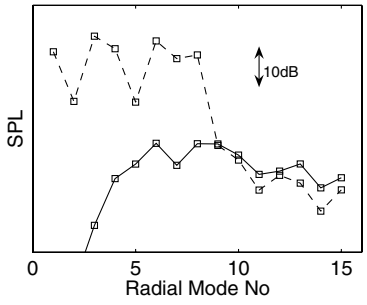

b) 3-D nonreflecting boundary conditions

Fig. 8 Amplitude of radial harmonics in $m = -6$ downstream of OGV; dashed line: transmitted (downstream) and solid line: reflected (upstream).

passing frequency and at different operating conditions for the same OGV geometry, yielding analogous results and confirming the effectiveness of the approach in eliminating spurious reflections from the boundaries in linear unsteady simulations.

VII. Conclusions

This paper presented an extension to viscous applications of a technique, developed by Hall et al. [10], to implement nonreflecting boundary conditions for the linear analysis of turbomachinery problems. Very efficient boundary conditions are achieved by using, throughout the computation, the dominant far-field acoustic eigenmodes precalculated for a swirling axisymmetric mean flow. The extra CPU and memory requirements are both negligible. Results show a large improvement in the reduction of the nonphysical reflection and an increase of the convergence rate. The implementation within a GMRES algorithm, originally developed for the linear Navier–Stokes solver, allows all aeroelastic analyses to benefit from the new treatment. Convergence can be enhanced further when both are used simultaneously.

Appendix: Model Problem Assumes Parallel Endwalls

Considering a steady flow $(\rho, \mathbf{U}, p)$, where $\mathbf{U} = (U_x, U_\theta, U_r)$, then the conservation form of the linearized entropy equation

$$\frac{\partial}{\partial t}(\rho s) + \nabla \cdot (\rho s \mathbf{U}) = 0$$

rearranged as

$$\rho\left(\frac{\partial s}{\partial t} + \mathbf{U} \cdot \nabla s\right) = -s \nabla \cdot (\rho \mathbf{U})$$

shows, after equalizing the right-hand side to zero (because of mass conservation), that the entropy is convected along a streamline.

If, however, the steady flowfield is taken to be a function of the radius r only, then,

$$\nabla \cdot (\rho \mathbf{U}) = r^{-1} \frac{\mathrm{d}}{\mathrm{d}r}[r\rho(r)U_r(r)]$$

which may be nonzero, leading to s either increasing or decreasing along a streamline.

To prevent this nonphysical behavior, it is necessary to set $U_r(r) = 0$, to give a physically sensible axisymmetric flowfield for the nonreflecting boundary-condition analysis.

Acknowledgments

This work was supported by Rolls-Royce, plc. The first author wishes to express his thanks to Alec Wilson from Rolls-Royce, plc. during the early stage of this work and to Sergio Campobasso for his help in the implementation of the new boundary-condition treatment inside the GMRES algorithm. The authors are also grateful to Davide Giacche from Cambridge University, who has kindly provided the last set of results.

References

[1] Adamczyk, J. J., Verdon, J. M., and Caspar, J. R., "Subsonic Flow Past an Oscillating Cascade with Steady Blade Loading—Basic Formulation," *Unsteady Aerodynamics*, edited by R. B. Kinney, Univ. of Arizona, Tucson, AZ, July 1975, pp. 827–851.

[2] Hall, K. C., and Crawley, E. F., "Calculation of Unsteady Flows in Turbomachinery Using the Linearized Euler Equations," *AIAA Journal*, Vol. 27, No. 6, 1989, pp. 777–787.

[3] Giles, M. B., "Nonreflecting Boundary Conditions for Euler Equation Calculation," *AIAA Journal*, Vol. 28, No. 12, Dec. 1990, pp. 2050–2058.

[4] Engquist, B., and Majda, A., "Absorbing Boundary Conditions for the Numerical Simulation of Waves," *Mathematics of Computation*, Vol. 31, No. 139, 1977, pp. 629–651.

[5] Saxer, A., and Giles, M. B., "Quasi-3-D Nonreflecting Boundary Conditions for Euler Equation Calculations," *Journal of Propulsion and Power*, Vol. 9, No. 2, 1993, pp. 263–271.

[6] Fan, S., and Lakshminarayana, B., "Time-Accurate Euler Simulation of Interaction of Nozzle Wake and Secondary Flow with Rotor Blade in an Axial Turbine Stage Using Nonreflecting Boundary Conditions," *Journal of Turbomachinery*, Vol. 118, Oct. 1996, pp. 663–677.

[7] Rowley, C. W., and Colonius, T., "Discretely Nonreflecting Boundary Conditions for Linear Hyperbolic Systems," *Journal of Computational Physics*, Vol. 157, No. 2, Jan. 2000, pp. 500–538.

[8] Grote, M. J., and Keller, J. B., "Exact Nonreflecting Boundary Conditions for the Time Dependent Wave Equation," *SIAM Journal on Applied Mathematics*, Vol. 55, No. 2, 1995, pp. 207–307.

[9] Tam, C. K. W., "Advances in Numerical Boundary Conditions for Computational Aeroacoustics," *Journal of Computational Acoustics*, Vol. 6, No. 4, 1998, pp. 377–402.

[10] Hall, K. C., Clark, W. S., and Lorence, C. B., "Non Reflecting Boundary Conditions for Linearized Unsteady Aerodynamic Calculations," 31st Aerospace Sciences Meeting and Exhibit, Reno, NV, AIAA Paper 93-0882, Jan. 1993.

[11] Fransson, T. H., and Verdon, J. M., "Panel Discussion on Standard Configurations for Unsteady Flow Through Vibrating Axial-Flow Turbomachinery Cascades," *Unsteady Aero-Dynamics, Aeroacoustics and Aeroelasticity and Propeller*, edited by H. M. Atassi, Springer–Verlag, New York, 1993, pp. 859–889.

[12] Moinier, P., and Giles, M. B., "Eigenmode Analysis for Turbomachinery Applications," *Journal of Propulsion and Power*, Vol. 21, No. 6, 2005, pp. 973–978.

[13] *Proceedings of the Third Computational Aeroacoustics (CAA) Workshop on Benchmark Problems*, NASA John H. Glenn Research Center at Lewis Field, Cleveland, OH, Nov. 1999.

[14] Tyler, J. M., and Sofrin, T. G., "Axial Flow Compressor Noise Studies," *S.A.E. Transactions*, Vol. 70, 1962, pp. 309–332.

[15] Campobasso, M. S., and Giles, M. B., "Effects of Flow Instabilities on the Linear Analysis of Turbomachinery," *Journal of Propulsion and Power*, Vol. 19, No. 19, Mar.–Apr. 2003, pp. 250–259.

[16] Moinier, P., "Algorithm Developments for an Unstructured Viscous Flow Solver," Ph.D. Thesis, Oxford Univ., Oxford, 1999.

[17] Duta, M. C., "The Use of the Adjoint Method for the Minimisation of Forced Response," Ph.D. Thesis, Oxford University, 2001.

[18] Wilson, A. G., "Application of CFD to Wake/Aerofoil Interation Noise —A Flat Plate Validation Case," AIAA Paper 2001-2135, 2001.

J. Oefelein
Associate Editor

This article has been cited by:

1. Jose Ramon Fernandez Aparicio, Adolfo Serrano. Turbine Tone Noise Prediction in High Speed Turbines Using a Linearized CFD Solver: Comparison with Measurements . [Abstract] [PDF] [PDF Plus]
2. Paruchuri Chaitanya, Pratibha Vellanki. 2021. Bayesian optimisation for low-noise aerofoil design with aerodynamic constraints. *International Journal of Aeroacoustics* **20**:1-2, 109-129. [Crossref]
3. Juan Manuel Gallardo, Adrián Sotillo, Óscar Bermejo. 2019. Study of the Effect of the Scatter of Acoustic Modes on Turbine Flutter. *Journal of Turbomachinery* **141**:10. . [Crossref]
4. Chaitanya C. Paruchuri, Pratibha Vellanki, Anuroopa Kalyan, John Coupland, Phillip Joseph. Low-noise OGV design for broadband noise using bayesian optimisation . [Citation] [PDF] [PDF Plus]
5. Nathan A. Wukie, Daniel Lindblad, Niklas Andersson. noisyduck: an open-source Python tool for computing eigenmode decompositions of duct flows . [Citation] [PDF] [PDF Plus]
6. Nathan A. Wukie, Paul D. Orkwis. Coarsening and filtering for absorbing layers in a discontinuous Galerkin method . [Citation] [PDF] [PDF Plus]
7. Nathan A. Wukie, Paul D. Orkwis, Daniel Lindblad, Niklas Andersson. Nonreflecting boundary conditions for the Euler equations in a discontinuous Galerkin discretization . [Citation] [PDF] [PDF Plus]
8. Daniel Lindblad, Nathan Wukie, Gonzalo Montero Villar, Niklas Andersson. A Nonreflecting Formulation for Turbomachinery Boundaries and Blade Row Interfaces . [Citation] [PDF] [PDF Plus]
9. Chaitanya Paruchuri, Phillip Joseph, Yijun Mao, Alexander G. Wilson. Prediction of turbulence-cascade interaction noise using modal approach . [Citation] [PDF] [PDF Plus]
10. José Ramón Fernández Aparicio, Adolfo Serrano. Tonal Noise Transmission through a Non-Axisymmetric Turbine OGV with Separated Flow: Prediction and Measurements . [Citation] [PDF] [PDF Plus]
11. Nathan A. Wukie, Mark Turner, Paul D. Orkwis. A Neumann pressure outlet boundary condition for compressible flows . [Citation] [PDF] [PDF Plus]
12. Nathan A. Wukie, Paul D. Orkwis, Mark G. Turner. A fully-implicit, Giles-type nonreflecting boundary condition in a DG-Chimera turbomachinery solver . [Citation] [PDF] [PDF Plus]
13. Chaitanya C. Paruchuri, John Coupland, Phillip Joseph. Airfoil geometry effects on turbulence interaction noise in cascades . [Citation] [PDF] [PDF Plus]
14. Davide Giacché, Liping Xu, John Coupland. 2014. Optimization of Bypass Outlet Guide Vane for Low Interaction Noise. *AIAA Journal* **52**:6, 1145-1158. [Abstract] [Full Text] [PDF] [PDF Plus]
15. Davide Giacche, Thomas P. Hynes, Stephane Baralon, John Coupland, Nicholas Humphreys, Peter Schwaller. Acoustic Optimization of Ultra-Low Count Bypass Outlet Guide Vanes . [Citation] [PDF] [PDF Plus]
16. Davide Giacche, Liping Xu, John Coupland. Multi-Disciplinary Multi-Objective Optimisation of Bypass OGV for Low Interaction Noise . [Citation] [PDF] [PDF Plus]
17. Davide Giacche, Liping Xu, John Coupland, Alexander G. Watson. 2011. Comparison Between Postprocessing Methods Applied to Rotor-Stator-Interaction Tone-Noise Problems. *AIAA Journal* **49**:6, 1214-1229. [Citation] [PDF] [PDF Plus]
18. Thomas Law, Roque Corral, José Ramón Fernández, Adolfo Serrano. Linear Viscous Eigenmode Analysis Within a Radially Varying Swirling Flow . [Citation] [PDF] [PDF Plus]